Materials Today Energy 37 (2023) 101377

Contents lists available at ScienceDirect

Materials Today Energy

journal homepage: www.journals.elsevier.com/materials-today-energy/

Hybrid surface coating layers comprising boron and phosphorous compounds on $LiNi_{0.90}Co_{0.05}Mn_{0.05}O_2$ cathode materials to ensure the reliability of lithium-ion batteries

Seung Ah Yu [a, b, g], Jae Kwon Seo [a, b, g], Jong Min Yun [a, b], Hayoung Park [c], Yonggoon Jeon [c], Jungwon Park [c, d, ***], Min-Sik Park [e, **], Young-Jun Kim [a, b, f, *]

[a] SKKU Advanced Institute of Nano Technology (SAINT), Sungkyunkwan University, Suwon 16419, Republic of Korea
[b] Department of Nano Science and Technology, Sungkyunkwan University, Suwon 16419, Republic of Korea
[c] School of Chemical and Biological Engineering, Seoul National University, Seoul 08826, Republic of Korea
[d] Center for Nanoparticle Research, Institute for Basic Science (IBS), Seoul National University, Seoul 08826, Republic of Korea
[e] Department of Advanced Materials Engineering for Information and Electronics, Kyung Hee University, Yongin 17104, Republic of Korea
[f] SKKU Institute of Energy Science and Technology (SIEST), Sungkyunkwan University, Suwon 16419, Republic of Korea

ARTICLE INFO

Article history:
Received 2 May 2023
Received in revised form
25 July 2023
Accepted 27 July 2023
Available online 2 August 2023

Keywords:
Ni-rich cathode materials
Hybrid surface coating
Lithium-ion batteries
Stability
Fast charging

ABSTRACT

High-energy lithium-ion batteries (LIBs) have undergone significant technological advancements in response to the expanding market for electric vehicles (EVs). Ni-rich layered cathode materials ($LiNi_xCo_{1-x-y}Mn_{1-x-y}O_2$, $x \geq 0.8$) are a viable option because of their high reversible capacity over 200 mAh/g. However, the inherent challenges of Ni-rich cathodes include the occurrence of residual lithium, side reactions, and structural instability. Herein, we propose a hybrid surface coating of boron and phosphorous on a $LiNi_{0.9}Co_{0.05}Mn_{0.05}O_2$ (NCM955) cathode material to minimise the side reactions and enhance the structural stability. The hybrid surface coating on NCM955 provides an excellent discharge capacity of 180 mAh/g at 5 C-rate compared to the bare NCM955 capacity of 159 mAh/g. After 300 cycles, the coated NCM955 retained 84% of its capacity, while the uncoated retained only 46%. The improvement can be attributed to the enhanced lithium-ion diffusion achieved through hybrid coating, as confirmed by impedance measurements and cyclic voltammetry analysis. TEM and XPS analyses were performed to validate the presence of the coating layer, confirming the presence of the desired material on the surface. This study provides practical guidance for designing highly reliable, high-capacity cathode materials for use in EV applications.

© 2023 Elsevier Ltd. All rights reserved.

1. Introduction

Over the past decade, lithium-ion batteries (LIBs) have attracted significant attention as the most reliable power source for electric vehicles (EVs) [1]. However, conventional cathode materials such as $LiCoO_2$ and $LiFePO_4$ are incapable of satisfying the requirements of high-energy LIBs [2–3]. In this respect, the Ni-rich layered cathode materials are considered the most competitive cathode material owing to their high capacity (>200 mAh/g) and low cost [4].

However, Ni-rich cathode materials still involve the following fundamental issues: i) side reactions with the electrolyte at the surface, and ii) structural degradation upon long-term cycling. These cathode materials contain a large amount of residual Li (i.e. LiOH and Li_2CO_3) on the surface [10]. This is not preferable because these can be oxidized conveniently by forming Li_2O and CO_2 gas at high-voltage operation, which causes a continuous loss of the Coulombic efficiency during cycling [11]. In addition, repeated cycling also induces irreversible phase transitions and micro-cracking of the cathode materials. This results in a significant performance reduction [5–7]. The most severe drawbacks are the decomposition of electrolytes through the side reactions with water in the electrolyte [8]. The hydrofluoric acid (HF) formed from

* Corresponding author.SKKU Advanced Institute of Nano Technology (SAINT), Sungkyunkwan University, Suwon 16419, Republic of Korea
** Corresponding author.
*** Corresponding author.Center for Nanoparticle Research, Institute for Basic Science (IBS), Seoul National University, Seoul 08826, Republic of Korea
E-mail addresses: jungwonpark@snu.ac.kr (J. Park), mspark@khu.ac.kr (M.-S. Park), yjkim68@skku.edu (Y.-J. Kim).
[g] Contributed equally.

https://doi.org/10.1016/j.mtener.2023.101377
2468-6069/© 2023 Elsevier Ltd. All rights reserved.

such side reactions between cathode materials and electrolyte can attack active materials. This accelerates the damage to the active material surface and facilitates transition metal dissolution [8–9].

To overcome these limitations, various structural modifications (e.g. coating and doping) have been adopted for these cathode materials to suppress the undesirable side reactions with electrolytes and the structural degradations during cycling [12,13]. Although various functional materials have been examined for effective surface stabilisation onto Ni-rich cathode materials, such fundamental issues have not been resolved fully.

Because conventional surface coatings are likely to increase the overpotential for interfacial charge-transfer reactions owing to their limited functionality [14], the selection of appropriate coating materials is crucial for improving the electrochemical performance of Ni-rich cathode materials. The coating materials should have a high ionic conductivity and should effectively reduce the residual Li on the surface [15,16]. Nonetheless, most studies have focused on surface coatings with a single coating material. However, by utilising two suitable coating materials, it may be feasible to achieve a high electrochemical performance.

In this study, we propose a hybrid surface coating process with phosphorus and boron on the surface of a $LiNi_{0.9}Co_{0.05}Mn_{0.05}O_2$ (NCM955) cathode material. We demonstrate the critical role of the hybrid coating layer in improving the rate capability and cycle performance of the MCN955 cathode material. H_3PO_4 and H_3BO_3 react with residual Li compounds on the surface of the cathode materials and transform into Li_3PO_4 (LPO) and $Li_2O{-}2B_2O_3$ (LBO) phases. Because both the resulting phases are known to be good ionic conductors [17,18] these can effectively facilitate interfacial charge transfer reactions at the surface of NCM955 cathode materials even at high current densities. Moreover, the hybrid coating layer can absorb moisture in the electrolyte. This is favourable for mitigating the generation of hydrofluoric (HF) acid in the electrolyte and improving the long-term cycling performance [14]. The residual Li on the surface of the cathode materials can be consumed during the hybrid surface coating process. Thus, we anticipate that the hybrid coating layer would be favourable for effectively suppressing the side reactions with the electrolyte and enhancing the Li^+ conductivity at the surface. This would enable a significant enhancement in the electrochemical performance of Ni-rich cathode materials.

2. Experiment

2.1. Synthesis of $LiNi_{0.90}Co_{0.05}Mn_{0.05}O_2$ (NCM955)

A layered precursor $Ni_{0.90}Co_{0.05}Mn_{0.05}(OH)_2$ was prepared using a co-precipitation method. Stoichiometric amounts of $NiSO_4{\cdot}6H_2O$, $CoSO_4{\cdot}7H_2O$, and $MnSO_4{\cdot}H_2O$ were dissolved in deionised water in the ratio 90:5:5. While the transition metal solution was continuously stirred, an NaOH solution was added dropwise as a precipitating agent. Moreover, an NH_4OH solution was added as a chelating agent into the continuously stirred-tank reactor. During the precipitation, the pH value of the reactor was adjusted to 10.75, and the temperature was 40 °C. The molar ratio of the overall metallic ions to the NH_4OH solution to the NaOH solution was 2:1:2. The synthesised precursor was dried, and the resulting powder was first mixed with LiOH (98%, Sigma Aldrich) in the molar ratio 1:1.03. Then, the mixture was calcined at 750 °C for 12 h under O_2 flow at a heating rate of 3 °C/min (denoted as bare).

2.2. Hybrid composite coating with Li_3PO_4 and $Li_2O{-}2B_2O_3$

LPO and LBO bi-functional coatings were prepared using a solution method. H_3PO_4 (Sigma Aldrich) and H_3BO_3 (Sigma Aldrich) were dissolved in ethanol. Subsequently, the NCM955 powder was added to the above solution and magnetically stirred at 300 rpm under 80 °C heat until the solvent ethanol evaporated completely. The product was dried in a vacuum oven at 80 °C and then, heated at 700 °C for 5 h in flowing O_2 gas. After the furnace was cooled to the room temperature, LPO/LBO-coated NCM955 powder was obtained (Scheme 1). The coated samples are denoted as P@B-NCM, P-NCM, and B-NCM. The chemical reactions are expressed as follows:

$$H_3PO_4 + 3LiOH \rightarrow Li_3PO_4 + 3H_2O,\ 2H_3PO_4 + 3Li_2CO_3 \rightarrow 2Li_3PO_4 + 3H_2O + 3CO_2$$

$$4H_3BO_3 + 2LiOH \rightarrow Li_2O{-}2B_2O_3 + 7H_2O,\ 4H_3BO_3 + Li_2CO_3 \rightarrow Li_2O{-}2B_2O_3 + 6H_2O + CO_2$$

$$H_3PO_4 + H_3BO_3 + 2LiOH \rightarrow Li_2O\text{-}BPO_4 + H_2O$$

2.3. Electrode preparation

To prepare the cathode electrodes, the homogeneous cathode slurry with a mass ratio of 94:3:3 (active material: carbon black (Super-P): polyvinylidene fluoride (PVDF)) dissolved in 1-methyl-2-pyrrolidone (NMP) solvent was cast onto aluminum foils (thickness = 15 μm). The electrodes were dried at 120 °C under vacuum, cut into 12 mm-diameter specimens, and roll-pressed. The loading level of cathode electrode was 15.5 ± 0.3 mg/cm^2, and the electrode density was fixed at 3.4 g/cc. A Li-metal disc (diameter = 14 mm, thickness = 200 μm) and 16 μm-thick polyethylene film were used as a half-cell counter electrode and separator, respectively. For the full cell, a commercial artificial graphite (LKP-G, Shanshan Technology) slurry with a mass ratio of

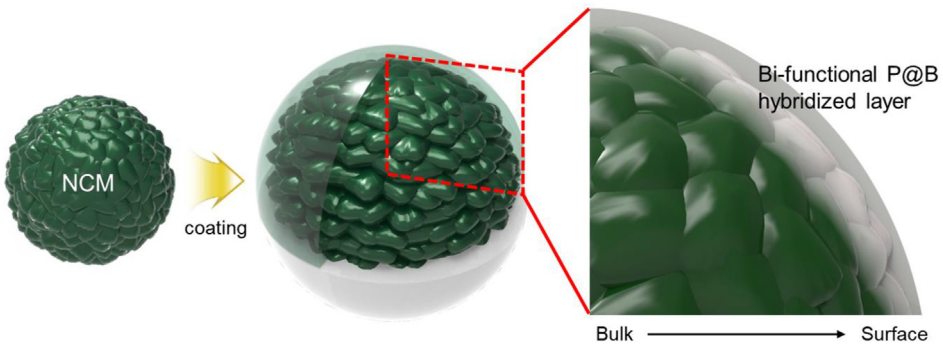

Scheme 1. (a) Schematic illustration of Li_3PO_4 and $Li_2O{-}2B_2O_3$ hybrid surface coating.

96:1:1.5:1.5 (active material: Super-P: SBR: CMC) was cast onto Cu foils (thickness = 18 μm) with an N/P ratio of 1.1. The electrolyte was formulated by combining ethylene carbonate, dimethyl carbonate, and ethyl methyl carbonate (in a volumetric ratio of 2:4:4), along with the inclusion of 1 wt% vinyl carbonate and 1 wt% difluorophosphate ($LiPO_2F_2$) as additives. The coin-type cells (CR2032) were assembled within a desiccated environment characterized by a dew point lower than −60 °C, ensuring optimal dryness conditions.

2.4. Material characterisation

The morphologies and microstructures of the synthesised powders were observed using scanning electron microscopy (SEM) (JSM-7600FM, JEOL) and cryo-transmission electron microscopy (cryo-TEM) (JEM-2100F, JEOL). The cross-sectional electrodes were prepared using a cross-sectional polisher (IB−19530CP, JEOL). The crystal structure of the prepared samples was characterised by powder X-ray diffraction (XRD) (Empyrean, PAN analytical) with Cu K_α radiation under incidence angles of 10°−80° at a scanning speed of 4.7°min. The surface compositions were determined by X-ray photoelectron spectroscopy (XPS) using a Sigma probe spectrometer (Thermo Scientific). Additionally, the elemental composition of coated cathode materials was determined using inductively coupled plasma optical emission spectroscopy (ICP-OES, Agilent 5100, Perkin Elmer). The particle hardness was measured using a micro-compression tester (MCT-W, Shimadzu).

2.5. Electrochemical measurements

Galvanostatic charge/discharge experiments were performed at a temperature of 25 °C utilising TOSCAT-3100 battery cycler (TOYO). The formation process consisted of two cycles that were measured at a constant current (CC) of 0.2 C with a CC−CV (constant voltage) charge protocol in the voltage range of 2.75−4.3 V vs. Li/Li^+. The discharge rate test was performed over several current rates (C-rate) of 0.2, 0.5, 1, 2, and 5 C (1 C = 205 mA/g) after charging at 0.2 C in the CC−CV mode using a 0.05 C cut-off. The cycling performance was examined at 0.5 C in the voltage window from 2.8 to 4.3 V vs. Li/Li^+ for 300 cycles at 25 °C and 60 °C, followed by CC-CV charging with a 0.05 C cut-off. Electrochemical impedance spectroscopy (EIS) was performed using a Biologic VSP-100 instrument in the frequency range 500 kHz−10 mHz at an amplitude of 10 mV. To compare the resistance components, EC-Lab software was used to fit the Nyquist plots. The lithium ion diffusion properties were analysed using the galvanostatic intermittent titration technique (GITT) and carried out on a battery cycler WBCS3000L (WonATech). For the GITT test, the cells were discharged at 0.1 C for 30 min. This was followed by a rest process under an open circuit for 2 h.

3. Results and discussion

The phase identification of the exposed NCM and P@B-NCM was conducted by powder XRD analysis, as shown in Fig. 1(a). The main diffraction patterns match well with the (003) and (104) planes of the typical layered α-$NaFeO_2$ structure (space group: R-3m) without impurity phase [19]. Moreover, narrow and clear peak splits of the (006)/(102) and (018)/(110) planes are evident in the patterns. This indicates that both materials have well-defined highly ordered hexagonal layered structures [20].

Meanwhile, the integrated intensity ratio ($I_{(003)}/I_{(104)}$) is known as an indicator of the degree of cation mixing [19]. Owing to the similar ionic radius of Li^+ (0.76 Å) and Ni^{2+} (0.69 Å), ionic interchange between Li^+ (Li slab) to Ni^{2+} (TM slab) sites occur straightforwardly. This would result in the degradation of electrochemical performance of layered cathode materials by the blocking of the Li^+ diffusion pathways [21]. An $I_{(003)}/I_{(104)}$ value significantly less than 1.2 indicates that Ni^{2+} migrates into the Li slab, which is contaminated with rock-salt domains [19]. Because most surface coatings increase the degree of cation mixing by consuming Li from the Li slab in bulk NCM, we investigated the effect of the hybrid surface coating on the crystal structure of NCM955. As shown in Table 1, P@B-NCM exhibited an $I_{(003)}/I_{(104)}$ value higher than 1.2. This implies that it maintained a low degree of cation mixing. This

Table 1
Lattice parameters and $I_{(003)}/I_{(104)}$ ratio of exposed and coated samples.

NCM955	a, b (Å)	c (Å)	I(003)/I(104)	c/a
Bare	2.872	14.197	2.22	4.943
Bare 2nd sintered	2.874	14.197	2.15	4.941
P	2.874	14.199	2.16	4.940
B	2.874	14.202	2.28	4.942
P@B	2.874	14.197	2.15	4.939

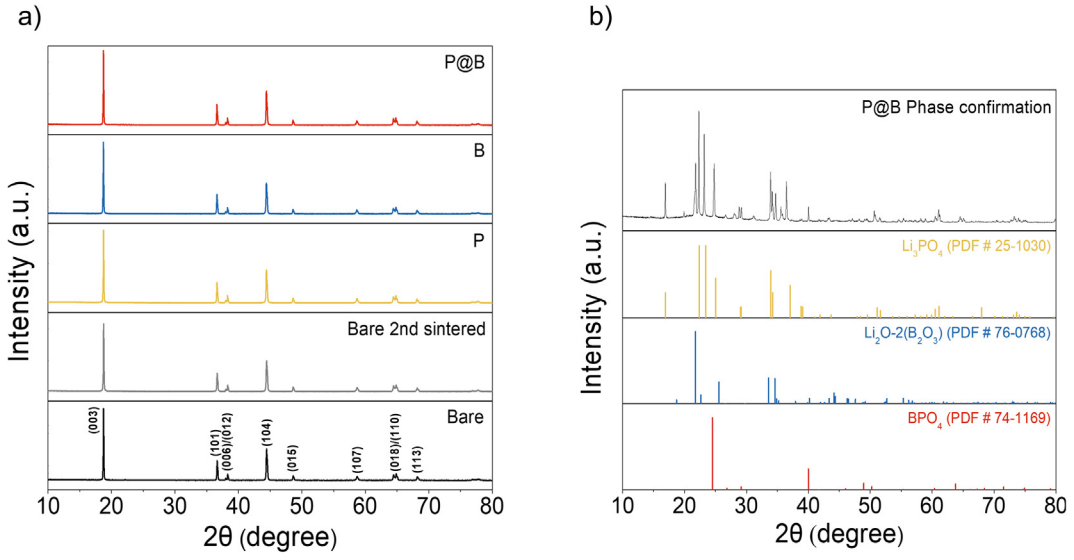

Fig. 1. (a) Powder XRD patterns of exposed and coated samples, and (b) P@B coating materials.

supports the assertion that the surface coating process does not affect the crystal structure of the host material (NCM955), and that only the residual Li (i.e. LiOH and Li_2CO_3) can participate in the formation of the hybrid coating layer. The characteristic peaks of the hybrid coating layer were not visible in the XRD pattern of P@B-NCM because of the low concentration of the coating materials. For phase confirmation, only the hybrid coating material was synthesised without NCM955 under similar conditions. The corresponding XRD pattern is presented in Fig. 1(b). The diffraction patterns match with those of LPO, LBO, and BPO_4. This reveals that

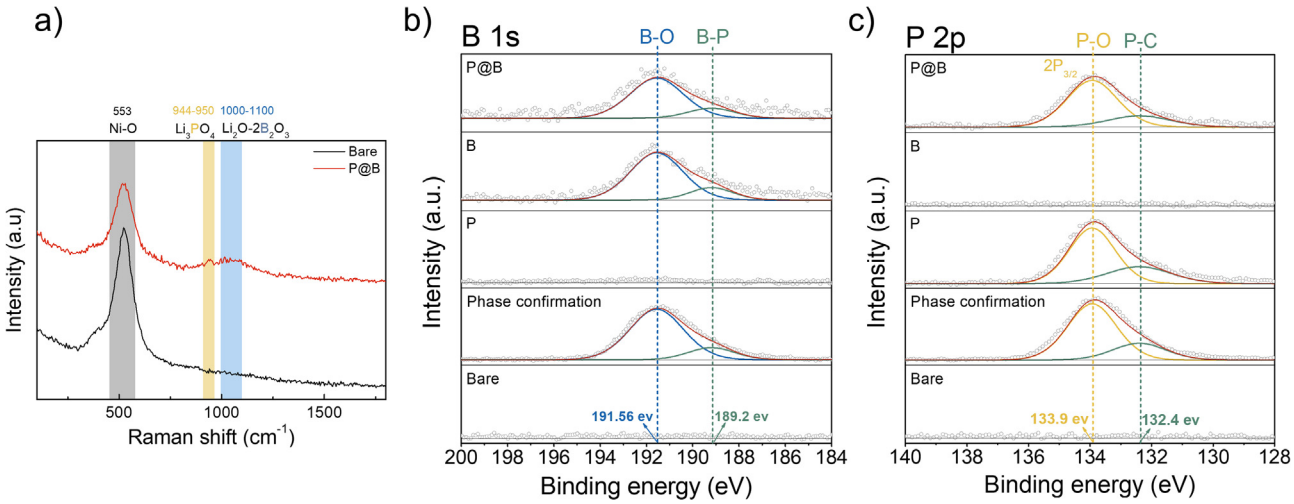

Fig. 2. (a) Raman, and (b) XPS spectra of B 1s and, (c) P 2p for exposed and P@B-NCM.

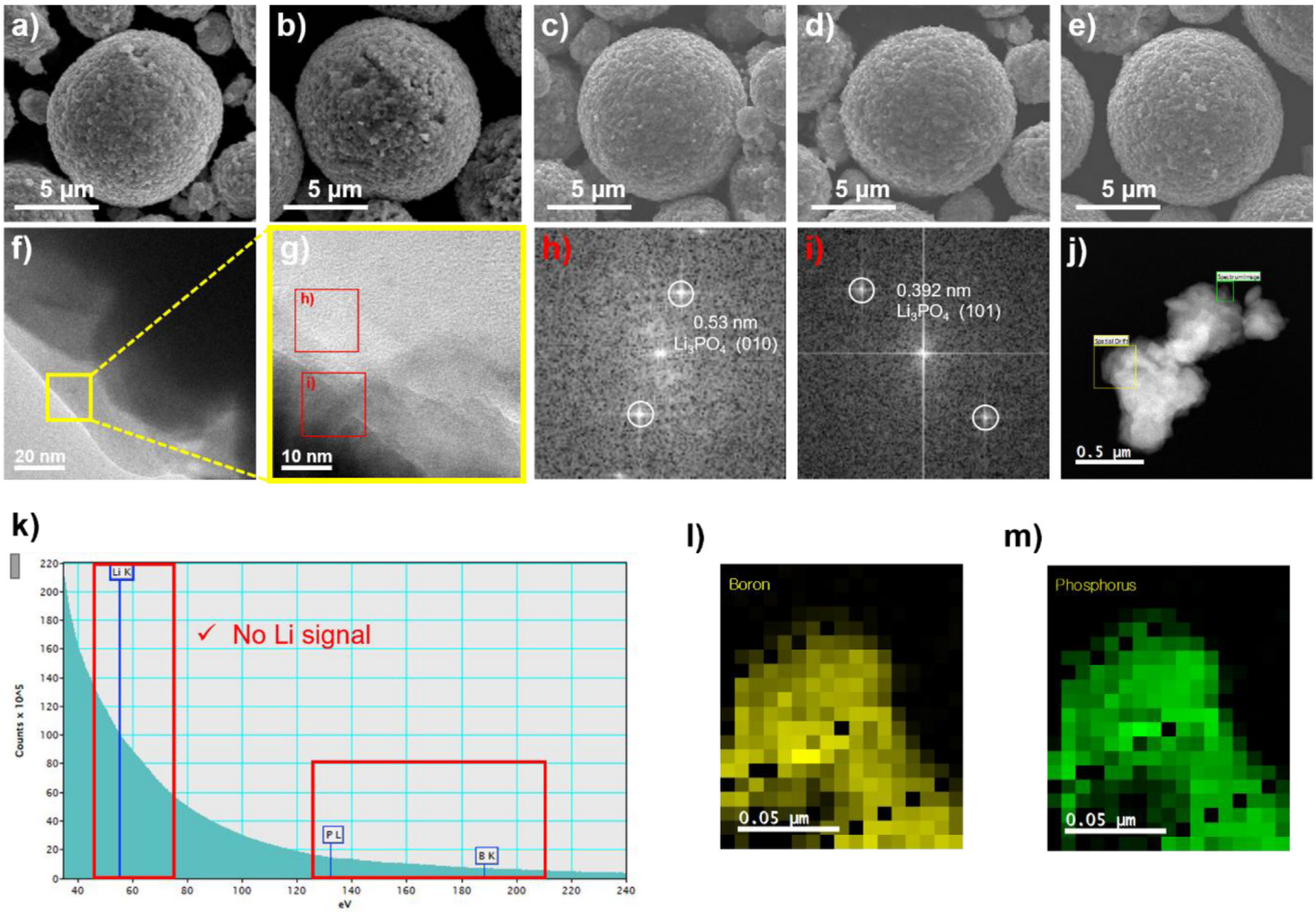

Fig. 3. FESEM images of (a) exposed, (b) exposed 2nd sintered, (c) P-NCM, (d) B-NCM, (e) P@B-NCM. HRTEM images of (f) P@B-NCM, FFT patterns of magnified (h, i) P@B coating layer. STEM image of (j) phase confirmation powder. EELS analysis of (k) bulk phase confirmation, (l) boron, and (m) phosphorous from selected area in (j).

the hybrid coating layer was composed of multiple phases including LPO, LBO, and BPO_4.

The Raman spectra of the exposed NCM and P@B-NCM are compared in Fig. 2(a). Strong Raman bands are expected to be observed around ~427, ~486, and ~553 cm. These are assigned to Ni–O, Co–O, and Mn–O vibrations originating from NCM955, respectively. Among those, the last peak of Raman spectroscopy is surely observed with extreme high portion Ni–O at 553 cm [22,23]. After the surface coating, P@B-NCM exhibited additional Raman bands. Here, a peak around 944–950 cm is associated with a symmetrical stretching of PO_4^{3-} in LPO [24,25]. Another peak near 1000–1100 cm indicates the presence of a well-defined diborate group of LBO [26,27].

The surface chemistry of P@B-NCM was inspected further using XPS. Fig. 2(b) and (c) presents the B 1s and P 2p spectra, respectively, after deconvolution based on 284.5 eV of C 1s excitation. After surface coating, there were no shifts in the binding energies of the major peaks in the spectra of exposed-NCM and P@B-NCM. This ensured that the ions were unaltered by the coating process [13]. Unlike exposed-NCM, strong signals are observed in both B 1s and P 2p spectra of P@B-NCM. This supports the assertion that an additional coating layer was introduced on the surface of NCM955. In the B 1s spectrum (Fig. 2(b)), the predominant peaks at the binding energies of 191.6 and 189.2 eV correspond to the B–O and B–P bonds, respectively [30]. The B 1s core levels are in good agreement with the values reported for B^{3+} in LBO [9,28,29]. In the deconvoluted P 2p spectra in Fig. 2(c), we observe characteristic peaks at 133.9 and 132.4 eV. These are mainly attributed to the P–O and P–C linkages, respectively [31–32]. These linkages could be derived from the reaction between residual Li and H_3PO_4. Note that a strong peak observed at 133.9 eV can be assigned to P^{5+} of LPO with a characteristic of a PO_4^{3-} tetrahedral chemical environment [30]. The XPS results are in good agreement with the phase identification based on the XRD analysis, as discussed above. Using ICP-OES, the contents of boron and phosphorus in the coated active materials were analysed (Table S1). For materials coated with either

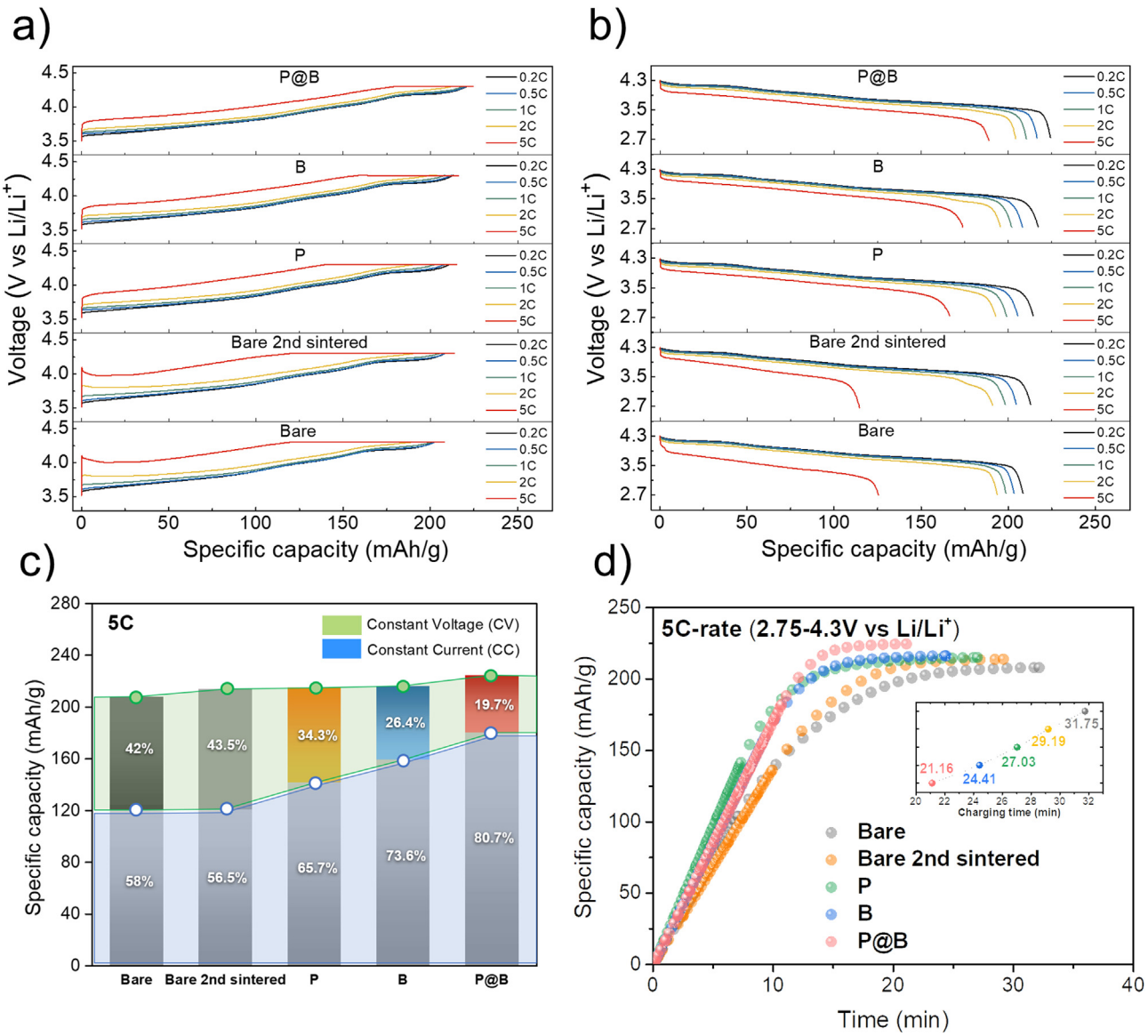

Fig. 4. Half-cell charge/discharge voltage profiles of exposed, exposed 2nd sintered, P-NCM, B-NCM, and P@B-NCM in a voltage range from 2.75 to 4.3 V vs. Li/Li^+: (a) galvanostatic charge curves and (b) galvanostatic discharge curves at different C-rates of 0.2, 0.5, 1, 2, and 5 C (1 C = 205 mA/g). (c) CC–CV charge proportion and (d) charging time curve of exposed, exposed 2nd sintered, P-NCM, B-NCM, and P@B-NCM at 5 C.

B or P, as well as those coated with both B and P, a slightly lower but comparable amount was verified compared to the initial mol% input after the synthesis. Regarding the coating layer where both B and P were added together, the total initial input was 0.80 mol%. The analysis results indicate a value of 0.74 mol%, suggesting that most of these elements were incorporated into the coating layer.

The morphologies and microstructures of the exposed NCM and P@B-NCM particles were investigated using SEM and TEM, as shown in Fig. 3. Cathode particles have spherical morphologies with an average diameter of approximately 10–12 μm. The exposed NCM particles were covered with residual Li composed of LiOH and Li_2CO_3. After the surface coating, an additional surface layer was introduced on the surface of the particles. It was presumed to be composed of LPO and LBO because of the chemical reactions between the residual Li and precursors (H_3BO_3 and H_3PO_4). The TEM observations verified the formation of a uniform hybrid coating layer (~20 nm-thick) on the surface of the particles after the coating process, as shown in Fig. 3(f) and (g). Based on the fast Fourier transform (FFT) patterns of the magnified surface regions of P@B-NCM, Fig. 3(h) and (i) demonstrate the crystal structures of LPO. Fig. 3(j) shows STEM images combined with the powder EELS analysis results (Fig. 3(k)) to identify the coexistence of the LPO and LBO phases. Even at low concentration of the hybrid coating layer, both P and B signals can be detected, as shown by the count-signal peaks in Fig. 3(k), and the presence of both B and P is further confirmed using elemental mapping, as depicted in Fig. 3(l) and (m). This demonstrates that the hybrid coating layer contained P and B compounds.

The galvanostatic charge and discharge tests were performed for all the cathodes at C-rates of 0.2, 0.5, 1, 2, and 5 C (1 C = 205 mA/g), as shown in Fig. 5(a) and (b), respectively. According to the initial voltage profiles recorded at a constant current of 0.2 C, the initial discharge capacities of the exposed-NCM and P@B-NCM cathodes were measured to be 208.4 and 224.2 mAh/g, respectively. For comparison, the H-NCM, P-NCM, and B-NCM cathodes were also tested under identical conditions. However, all the samples exhibited smaller discharge capacities than the P@B-NCM cathode. The initial Coulombic efficiencies of the exposed-NCM and P@B-NCM cathodes were also estimated to be 89.2% and 93.7%, respectively. The higher discharge capacity of the P@B-NCM cathode could be attributed to the enhanced Li^+ kinetics at the surface by integrating a hybrid layer composed of highly conductive LPO and LBO and by reducing the amount of residual Li on the surface [8,28,30].

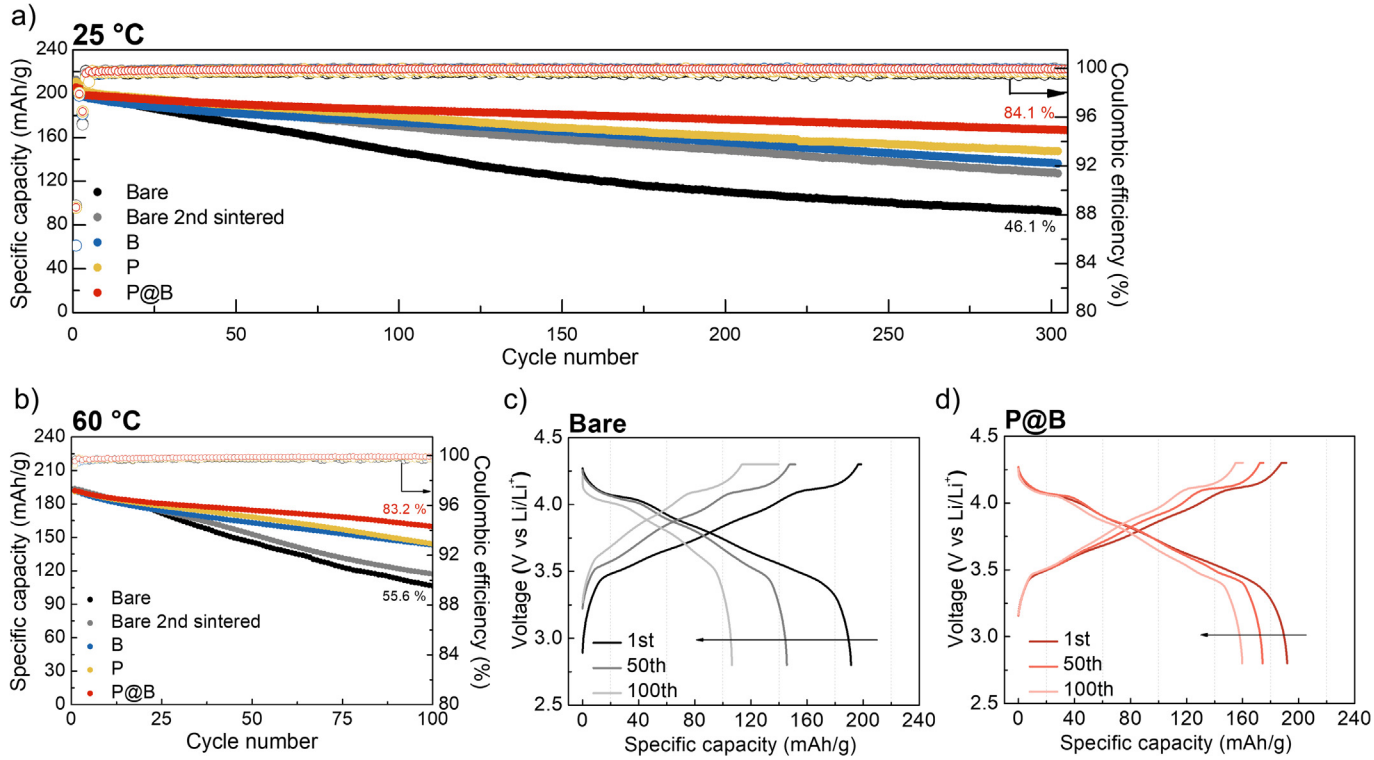

Fig. 5. Full cell cycle performance at (a) room temperature, and (b) 60 °C at 0.5 C in a voltage range of 2.8–4.3 V. Specific charge/discharge voltage profiles of (c) exposed and (d) P@B-NCM at 60 °C.

Table 2
Capacity retention for exposed, exposed 2nd sintered, P-NCM, B-NCM, and P@B-NCM samples after 300 cycles at 0.5 C in the range 2.8–4.3 V.

	Temperature (°C)	Discharge capacity (mAh/g)			Capacity retention (%)	Temperature (°C)	Discharge capacity (mAh/g)			Capacity retention (%)
		0.1C formation	0.5C 1st	0.5C 300th			0.1C formation	0.5C 1st	0.5C 100th	
Bare	25	206.60	199.71	92.14	46.1	60	197.20	191.42	106.50	55.6
Bare 2nd sintered	25	210.00	201.10	127.09	63.2	60	193.24	193.67	117.18	60.5
B	25	204.24	197.47	136.15	68.9	60	197.55	191.81	143.00	74.5
P	25	209.18	202.84	147.39	72.6	60	197.56	191.11	144.08	75.3
P@B	25	204.81	198.47	166.93	84.1	60	198.20	191.87	159.73	83.2

As anticipated, the thin hybrid coating layer functioned as an artificial cathode–electrolyte interface (CEI). It prevented direct contact between the cathode material and electrolyte for mitigating the solid–liquid reaction and enhancing the mechanical stability of the cathode material. The formation of the uniform hybrid coating layer significantly improved the initial Coulombic efficiency of the P@B-NCM cathode. This was because unnecessary irreversible phase transformations could be mitigated effectively at the surface by restraining the Li^+ consumption in the bulk NCM structure. Moreover, it passivated the cathode material through side reactions during liquid–electrolyte curing. To examine the rate capability of the cathode materials, the cells were galvanostatically charged and discharged at 0.2, 0.5, 1, 2, and 5 C (1 C = 205 mA/g), as depicted in Fig. 4(a) and (b). P@B-NCM exhibited a superior rate capability compared with the other cathode materials. In practice, P@B-NCM showed a significantly higher reversible capacity (188.2 mAh/g) than that of exposed-NCM (125.0 mAh/g) even at a high C-rate of 5 C. These results are consistent with those of the charging rate test. In particular, the capacity contributions of CC charging were estimated to be 120.7 and 180.2 mA/g for the exposed-NCM and P@B-NCM cathodes, respectively, corresponding to their total charge capacities of 58% and 80.3%, respectively. Note that the Li^+ conductive hybrid coating layer composed of LPO, LBO, and Li_2O-BPO_4 (LBPO) facilitated Li^+ transport at the interface by reducing the activation energy for Li^+ migration. This resulted in an enhanced rate capability [33]. Moreover [8,14,30] the formation of LPO, LBO, and LBPO as a hybrid coating layer effectively consumed the insulating residual Li on the surface. Thereby, the polarisation could be decreased for Li^+ transport even at a high current density [12]. The P@B-NCM cathode exhibited relatively marginal overpotentials as the C-rate increased, as shown in Fig. 4(a and b). Therefore, the introduction of a hybrid coating layer would be favourable for enhancing the Li^+ kinetics with the effective elimination of the residual Li.

To examine the feasibility of the P@B-NCM cathode, full cells were assembled using commercial anodes with an N/P ratio of 1.1. The full-cells were cycled at 0.1C (2 cycles) for formation and 0.5 C (300 cycles) in the voltage range of 2.8–4.3 V at room temperature.

A comparison of Fig. 5(c) and (d) reveals that there was no significant difference in the voltage profiles of the full cells assembled with the exposed-NCM and P@B-NCM cathodes. This indicates that the hybrid surface coating does not significantly affect the electrochemical behavior of the Ni-rich cathode materials.

The full-cell with P@B-NCM cathode showed a stable cycling performance up to 300 cycles with a high capacity retention of 84.1%. This value is higher than that of the full-cell with the exposed-NCM cathode (46.1%). The capacity retentions of the full-cells with the P-NCM and B-NCM cathodes were estimated to be 72.6% and 68.9%, respectively (Table 2). These considerable improvements in cyclability are attributed mainly to the hybrid coating layer. It suppresses side reactions and enhances Li^+ conductivity (Fig. S1 and Explanation).

Furthermore, the cycling performance of full cells was also examined at an elevated temperature (60 °C) with a 0.5 C for 100 cycles. Even at a high temperature of 60 °C, the full-cell with P@B-NCM cathode maintained a capacity retention of 83.2% after 100

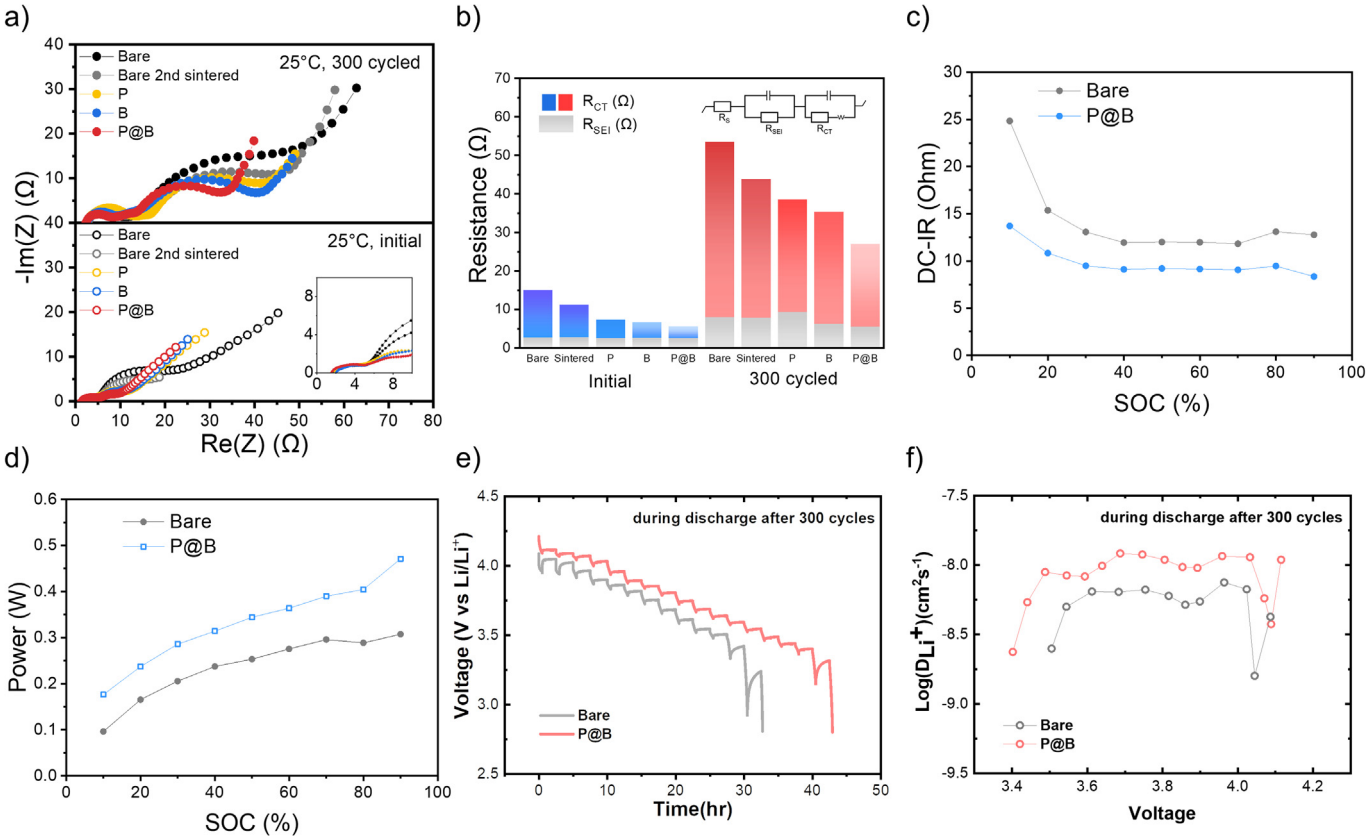

Fig. 6. (a) EIS spectra Nyquist plots (b) resulting resistance parameters for full cells made of exposed, exposed 2nd sintered, P-NCM, B-NCM, and P@B-NCM samples before and after 300 cycles with equivalent circuit used to model obtained impedance spectra. (c) DC-IR, (d) discharge power of full cells after 300 cycles measured by HPPC according to SOC. (e) Voltage profiles during GITT measurements and the corresponding (f) Li^+ diffusion coefficient during the discharge after 300 cycles of exposed NCM955 and P@B-NCM955. Galvanostatic current pulses are applied with current rates of 0.1 C for 30 min, followed by a 2 h rest period.

cycles, whereas the full-cell with exposed-NCM showed a capacity retention of 55.6% (Table 2). This reveals that the hybrid coating layer also enhanced the thermal resistance of Ni-rich cathode materials by inhibiting the direct contact of the cathode with the electrolyte and scavenging HF. This, in turn, resulted in an enhanced cycling stability even at a high temperature [9,14].

The Li^+ transport behaviors of the exposed NCM and P@B-NCM were investigated to identify the critical role of the coating layer, using the EIS, HPPC, and GITT techniques (Fig. 6). The Nyquist plots of the exposed NCM and P@B-NCM cathodes were obtained and fitted with an equivalent circuit as shown in the inset of Fig. 6(b). The measured EIS spectra consist of multiple components: i) Ohmic resistance (R_s), which mainly originated from the contact with the electrolyte; ii) a semicircle in the high-frequency region corresponding to the surface film resistance of the solid-electrolyte interphase (SEI) (R_{SEI}); and iii) a semicircle in the intermediate-frequency region representing the charge transfer resistance (R_{ct}) at the interface. Based on the Nyquist plots depicted in Fig. 6(a), it is feasible to evaluate the initial electrolyte resistance, which serves as an indicator of the degree to which Li^+ can effectively conduct across the region in contact with the electrolyte. The decreased resistance of the electrolyte, specifically referred to as R_{sol}, can be considered an indication of enhanced Li^+ mobility. Furthermore, the increased conductivity of Li^+ in a coating material can be noticed through the discernible change in the slope of the Nyquist plot at low frequencies, which occurs after 300 cycles.

The exposed NCM cathode showed a rapid increase in the R_{SEI} and R_{ct} values after 300 cycles. This is consistent with the DC-IR (direct current-internal resistance) results (Fig. 6(c) and (d)). This was attributed mainly to the severe capacity reduction of the exposed NCM cathode owing to the insulating residual Li and irreversible phase transformations during cycling. As a result of the significant phase transformation by resistance increase, repeated volume contraction and expansion ended up physical particle collapse of the exposed NCM compared to majority of intact particle of P@B-NCM (Figs. S2 and S3).

In the case of the P@B-NCM cathode, the R_{SEI} and R_{ct} values were relatively smaller than those of the exposed NCM cathode after cycling, with smaller DC-IR results. These results can be interpreted as the synergistic effects of the Li^+-conductive hybrid coating layer. Here, Li_3PO_4 suppresses the dissolution of transition metals by scavenging HF, and $Li_2O{-}2B_2O_3$ reduces the activation energy for Li^+ transport.

To clarify the positive effects of hybrid coating layer, the Li^+ diffusion coefficients of the exposed-NCM and P@B-NCM cathodes were calculated from the GITT profiles. The results were plotted as a function of voltage [34]. It is apparent that the P@B-NCM cathode maintained high values of Li^+ diffusivity compared with the exposed-NCM cathode. This can be reasonably explained by the reduced lattice distortions, which are mainly caused by the H1−H2 and H2−H3 phase transitions as illustrated in Fig. 6(f).

The integration of the strong B−O bonds on the surface of the cathode material induces effective surface stabilisation. This is more favourable for the Li^+ transport and enhances the mechanical strength during cycling [8]. Compared with the GITT profiles, the overpotential of P@B-NCM could be reduced effectively after the hybrid surface coating. This indicated the enhancement of the Li^+ diffusion behavior even after 300 cycles [35].

4. Conclusions

In this study, we demonstrated the favourable effects of a hybrid surface coating with bifunctionality for suppressing side reactions at the surface and enhancing the structural integrity of Ni-rich cathode materials. The residual Li can be utilised as a source for the formation of a thin Li^+ conductive layer composed of Li_3PO_4 and $Li_2O{-}2B_2O_3$ via chemical reactions with H_3BO_3 and H_3PO_4 during the coating process. This hybrid coating layer passivates the Ni-rich cathode material from HF attack and enhances the Li^+ mobility. We demonstrated the critical role of the hybrid coating layer in improving the rate capability and cycling performance of Ni-rich cathode materials. In practice, the P@B-NCM cathode exhibited a superior capacity retention of 80.3% even at a high current density of 5.0 C. It also showed a stable cycling performance up to 300 cycles, with a high capacity retention of 84%. Such improvements are mainly attributed to the bifunctionality of the hybrid coating layer on the surface of the Ni-rich cathode materials. We anticipate that the current issues with Ni-rich cathode materials can be resolved through a facile bifunctional hybrid surface coating to develop advanced LIBs.

Credit author statement

Seung Ah Yoo: Conceptualization, Investigation, Data curation, Validation, Writing original draft.
Jae Kwon Seo: Investigation, Visualization.
Jong Min Yun: Conceptualization, Investigation.
Hayoung Park: Investigation.
Yonggoon Jeon: Investigation.
Jungwon Park: Investigation, Editing.
Min-Sik Park: Review and editing, Validation.
Young-Jun Kim: Supervision, Funding acquisition, Project administration, Writing − review and editing, Validation.

Declaration of competing interest

The authors declare the following financial interests/personal relationships which may be considered as potential competing interests:

Young-Jun Kim reports financial support was provided by National Research Foundation of Korea.

Data availability

Data will be made available on request.

Acknowledgments

This work was supported by the National Research Foundation of Korea (NRF) grant funded by the Korea government (MSIT) (No.NRF-2021M3H4A1A02045962).

Appendix A. Supplementary data

Supplementary data to this article can be found online at https://doi.org/10.1016/j.mtener.2023.101377.

References

[1] A. Manthiram, A reflection on lithium-ion battery cathode chemistry, Nat. Commun. 11 (1) (2020) 1−9.
[2] P. Guan, L. Zhou, Z. Yu, Y. Sun, Y. Liu, F. Wu, Y. Jiang, D. Chu, Recent progress of surface coating on cathode materials for high-performance lithium-ion batteries, J. Energy Chem. 43 (2020) 220−235.
[3] W. Liu, F. Gao, Y. Zang, J. Qu, J. Xu, S. Ji, Y. Huo, J. Qiu, Boosting cycle stability of NCM811 cathode material via 2D Mg-Al-LDO nanosheet coating for lithium-ion battery, J. Alloys Compd. 867 (2021) 159079.
[4] L. Liang, G. Hu, F. Jiang, Y. Cao, Electrochemical behaviours of SiO_2-coated $LiNi_{0.8}Co_{0.1}Mn_{0.1}O_2$ cathode materials by a novel modification method, J. Alloys Compd. 657 (2016) 570−581.
[5] N. Yabuuchi, K. Yoshii, S.-T. Myung, I. Nakai, S. Komaba, Detailed studies of a high-capacity electrode material for rechargeable batteries, $Li_2MnO_3{-}LiCo_{1/3}Ni_{1/3}Mn_{1/3}O_2$, J. Am. Chem. Soc. 133 (12) (2011) 4404−4419.

[6] C. Liu, F. Li, L.-P. Ma, Hui-Mi Cheng, Advanced materials for energy storage, Adv. Mater. 22 (2010) E28–E62.

[7] A. Chakraborty, S. Kunnikuruvan, S. Kumar, B. Markovsky, D. Aurbach, M. Dixit, D.T. Major, Layered cathode materials for lithium-ion batteries: review of computational studies on $LiNi_{1-x-y}Co_xMn_yO_2$ and $LiNi_{1-x-y}Co_xAl_yO_2$, Chem. Mater. 32 (3) (2020) 915–952.

[8] J.S. Chae, S.-B. Yoon, W.-S. Yoon, Y.-M. Kang, S.-M. Park, J.-W. Lee, K.C. Roh, Enhanced high-temperature cycling of Li_2O–$2B_2O_3$-coated spinel-structured $LiNi_{0.5}Mn_{1.5}O_4$ cathode material for application to lithium-ion batteries, J. Alloys Compd. 601 (2014) 217–222.

[9] D. Wang, X. Li, Z. Wang, H. Guo, X. Chen, X. Zheng, Y. Xu, J. Ru, Multifunctional Li_2O-$2B_2O_3$ coating for enhancing high voltage electrochemical performances and thermal stability of layered structured $LiNi_{0.5}Co_{0.2}Mn_{0.3}O_2$ cathode materials for lithium ion batteries, Electrochim. Acta 174 (2015) 1225–1233.

[10] H.-J. Noh, S. Youn, C.S. Yoon, Y.-K. Sun, Comparison of the structural and electrochemical properties of layered Li $[Ni_xCo_yMn_z]O_2$ (x=1/3, 0.5, 0.6, 0.7, 0.8 and 0.85) cathode material for lithium-ion batteries, J. Power Sources 233 (2013) 121–130.

[11] D.-H. Cho, C.-H. Jo, W. Cho, Y.-J. Kim, H. Yashiro, Y.-K. Sun, S.-T. Myung, Effect of residual lithium compounds on layer Ni-rich Li $[Ni_{0.7}Mn_{0.3}]$ O_2, J. Electrochem. Soc. 161 (6) (2014) A920.

[12] T. Sattar, S.-J. Sim, B.-S. Jin, H.-S. Kim, Dual function Li-reactive coating from residual lithium on Ni-rich NCM cathode material for Lithium-ion batteries, Sci. Rep. 11 (1) (2021) 1–9.

[13] K. Park, J.-H. Park, S.-G. Hong, B. Choi, S.-W. Seo, J.-H. Park, K. Min, Enhancement in the electrochemical performance of zirconium/phosphate bifunctional coatings on $LiNi_{0.8}Co_{0.15}Mn_{0.05}O_2$ by the removal of Li residuals, Phys. Chem. Chem. Phys. 18 (42) (2016) 29076–29085.

[14] C.-H. Jo, D.-H. Cho, H.-J. Noh, H. Yashiro, Y.-K. Sun, S.T. Myung, An effective method to reduce residual lithium compounds on Ni-rich Li $[Ni_{0.6}Co_{0.2}Mn_{0.2}]$ O_2 active material using a phosphoric acid derived Li_3PO_4 nanolayer, Nano Res. 8 (5) (2015) 1464–1479.

[15] X. Yu, J. Bates, G. Jellison, F. Hart, A stable thin-film lithium electrolyte: lithium phosphorus oxynitride, J. Electrochem. Soc. 144 (2) (1997) 524.

[16] A.T. Appapillai, A.N. Mansour, J. Cho, Y. Shao-Horn, Microstructure of $LiCoO_2$ with and without "$AlPO_4$" nanoparticle coating: combined STEM and XPS studies, Chem. Mater. 19 (23) (2007) 5748–5757.

[17] W. Soppe, F. Aldenkamp, H. Den Hartog, The structure and conductivity of binary and ternary glasses $(B_2O_3)_{1-xy}$ $(Li_2O)_x$ $(Li_2Cl_2)_y$, J. Non Cryst. Solids 91 (3) (1987) 351–374.

[18] M. Eddrief, P. Dzwonkowski, C. Julien, M. Balkanski, The AC conductivity in B_2O_3-Li_2O films, Solid State Ion. 45 (1–2) (1991) 77–82.

[19] T. Weigel, F. Schipper, E.M. Erickson, F.A. Susai, B. Markovsky, D. Aurbach, Structural and electrochemical aspects of $LiNi_{0.8}Co_{0.1}Mn_{0.1}O_2$ cathode materials doped by various cations, ACS Energy Lett. 4 (2) (2019) 508–516.

[20] J. Li, Z. Liu, Y. Wang, R. Wang, Investigation of facial B_2O_3 surface modification effect on the cycling stability and high-rate capacity of $LiNi_{1/3}Co_{1/3}Mn_{1/3}O_2$ cathode, J. Alloys Compd. 834 (2020) 155150.

[21] M. Wang, R. Zhang, Y. Gong, Y. Su, D. Xiang, L. Chen, Y. Chen, M. Luo, M. Chu, Improved electrochemical performance of the $LiNi_{0.8}Co_{0.1}Mn_{0.1}O_2$ material with lithium-ion conductor coating for lithium-ion batteries, Solid State Ion. 312 (2017) 53–60.

[22] C. Lee, Y. Yokoyama, Y. Kondo, Y. Miyahara, T. Abe, K. Miyazaki, Mechanism of the loss of capacity of $LiNiO_2$ electrodes for use in aqueous Li-ion batteries: unveiling a fundamental cause of deterioration in an aqueous electrolyte through in situ Raman observation, ACS Appl. Mater. Interfaces 12 (50) (2020) 56076–56085.

[23] L. Song, X. Li, Z. Xiao, J. Du, Z. Cao, A. Li, H. Zhu, Thermo-electrochemical study of co-modified Li_2O-$2B_2O_3$-$(LiNi_{0.5}Co_{0.2}Mn_{0.3})_{0.98}Zr_{0.02}O_2$ cathode material, Ionics 26 (2) (2020) 673–681.

[24] L. Popović, B. Manoun, D. De Waal, M. Nieuwoudt, J. Comins, Raman spectroscopic study of phase transitions in Li_3PO_4, J. Raman Spectrosc. 34 (1) (2003) 77–83.

[25] Y. Matsuda, N. Kuwata, T. Okawa, A. Dorai, O. Kamishima, J. Kawamura, In situ Raman spectroscopy of Li_xCoO_2 cathode in $Li/Li_3PO_4/LiCoO_2$ all-solid-state thin-film lithium battery, Solid State Ion. 335 (2019) 7–14.

[26] H.S. Kang, P. Santhoshkumar, J.W. Park, G.S. Sim, M. Nanthagopal, C.W. Lee, Glass ceramic coating on $LiNi_{0.8}Co_{0.1}Mn_{0.1}O_2$ cathode for Li-ion batteries, Kor. J. Chem. Eng. 37 (8) (2020) 1331–1339.

[27] A.K. Yadav, P. Singh, A review of the structures of oxide glasses by Raman spectroscopy, RSC Adv. 5 (83) (2015) 67583–67609.

[28] S. Tan, L. Wang, L. Bian, J. Xu, W. Ren, P. Hu, A. Chang, Highly enhanced low temperature discharge capacity of $LiNi_{1/3}Co_{1/3}Mn_{1/3}O_2$ with lithium boron oxide glass modification, J. Power Sources 277 (2015) 139–146.

[29] X. Zhu, X. Ma, R.N. Ali, B. Zheng, M. Song, A novel and efficient method for the synthesis of strong fluorescence and long afterglow BPO_4 phosphors, Ceram. Int. 48 (6) (2022) 8209–8215.

[30] W. Ge, H. Wang, Z. Xie, X. Li, M. Qu, G. Peng, Amorphous 0.035 Li_2O-BPO_4 coating for enhanced electrochemical performance of Li $[Ni_{0.5}Co_{0.2}Mn_{0.3}]O_2$ cathode material, J. Alloys Compd. 693 (2017) 606–614.

[31] S. Gopi, V. Selvamani, K. Yun, MoS2 decoration followed by P inclusion over Ni-Co bimetallic metal–organic framework-derived heterostructures for water splitting, Inorg. Chem. 60 (14) (2021) 10772–10780.

[32] R. Li, Z. Wei, X. Gou, W. Xu, Phosphorus-doped graphene nanosheets as efficient metal-free oxygen reduction electrocatalysts, RSC Adv. 3 (25) (2013) 9978–9984.

[33] Z.-F. Tang, R. Wu, P.-F. Huang, Q.-S. Wang, C.-H. Chen, Improving the electrochemical performance of Ni-rich cathode material $LiNi_{0.815}Co_{0.15}Al_{0.035}O_2$ by removing the lithium residues and forming Li_3PO_4 coating layer, J. Alloys Compd. 693 (2017) 1157–1163.

[34] W. Zhang, L. Liang, F. Zhao, Y. Liu, L. Hou, C. Yuan, Ni-rich $LiNi_{0.8}Co_{0.1}Mn_{0.1}O_2$ coated with Li-ion conductive Li_3PO_4 as competitive cathodes for high-energy-density lithium ion batteries, Electrochim. Acta 340 (2020) 135871.

[35] C. Zhang, J. Wan, Y. Li, S. Zheng, K. Zhou, D. Wang, D. Wang, C. Hong, Z. Gong, Y. Yang, Restraining the polarization increase of Ni-rich and low-Co cathodes upon cycling by Al-doping, J. Mater. Chem. 8 (14) (2020) 6893–6901.